



This is the accepted manuscript made available via CHORUS. The article has been published as:

Phase diagram of the math xmlns="http://www.w3.org/1998/Math/MathML">mrow>mi >v/mi>mo>=/mo>mn>2/mn>/mrow>/math> quantum Hall state in bilayer graphene

Udit Khanna, Ke Huang, Ganpathy Murthy, H. A. Fertig, Kenji Watanabe, Takashi Taniguchi, Jun Zhu, and Efrat Shimshoni

Phys. Rev. B **108**, L041107 — Published 26 July 2023

DOI: 10.1103/PhysRevB.108.L041107

Phase diagram of the $\nu = 2$ quantum Hall state in bilayer graphene

Udit Khanna, ¹ Ke Huang, ² Ganpathy Murthy, ³ H. A. Fertig, ⁴ Kenji Watanabe, ⁵ Takashi Taniguchi, ⁶ Jun Zhu, ² and Efrat Shimshoni ¹

¹Department of Physics, Bar-Ilan University, Ramat Gan 52900, Israel

²Department of Physics, The Pennsylvania State University, University Park, Pennsylvania 16802, USA

³Department of Physics and Astronomy, University of Kentucky, Lexington, Kentucky 40506, USA

⁴Department of Physics, Indiana University, Bloomington, Indiana 47405, USA

⁵Research Center for Functional Materials, National Institute for Materials Science, 1-1 Namiki, Tsukuba 305-0044, Japan

⁶International Center for Materials Nanoarchitectonics,
National Institute for Materials Science, 1-1 Namiki, Tsukuba 305-0044, Japan

Bilayer graphene exhibits a rich phase diagram in the quantum Hall regime, arising from a multitude of internal degrees of freedom, including spin, valley, and orbital indices. The variety of fractional quantum Hall states between filling factors $1 < \nu \le 2$ suggests, among other things, a quantum phase transition between valley-unpolarized and polarized states at a perpendicular electric field D^* . We find the behavior of D^* with ν changes markedly as B is reduced. At $\nu=2$, D^* may even vanish when B is sufficiently small. We present a theoretical model for lattice-scale interactions which explains these observations; surprisingly, both repulsive and attractive components in the interactions are required. Within this model we analyze the nature of the $\nu=2$ state as a function of the magnetic and electric fields, and predict that valley-coherence may emerge for $D \sim D^*$ in the high B regime. This suggests the system supports Kekule bond-ordering, which could in principle be verified via STM measurements.

Introduction. The quantum Hall (QH) regime of twodimensional electronic systems with several internal degrees of freedom presents an intriguing many-body problem, where the interplay of interactions and degenerate Landau levels (LLs) often leads to a multitude of possible ground states [1–5]. Graphene and its few-layer variants offer compelling material platforms to explore this interplay due to their rich Landau spectrum, involving approximate SU(4) symmetry in spin and valley sectors, as well as relatively high mobilities and wide gate tunability [6–12].

Graphene systems, uniquely, support QH phases around charge neutrality, whose nature has been investigated extensively. Previous theoretical studies [13– 18 have clarified that the order underlying the ground state depends crucially on lattice-scale corrections to the (long-range) Coulomb interaction, which reduce the valley SU(2) symmetry to U(1)× \mathbb{Z}_2 . The precise form of these corrections is unclear and may depend on the device configuration. In light of this, the standard approach, introduced by Kharitonov [14–16], is to include phenomenological terms consistent with the symmetry. Conventionally, these terms are assumed to be independent of the magnetic field (B) and have a range of order the lattice constant, which is much smaller than the magnetic length $[\ell = \sqrt{\hbar/eB}]$. In what follows we will refer to this as the orthodox model (OM) of the lattice scale interactions.

Generally, the OM has been in accordance with experimental observations. In particular, for the $\nu=0$ phase of monolayer and bilayer graphene (MLG and BLG respectively), this model supports the interpretation of transport [19–23] and magnon transmission [24–26] experiments in terms of a magnetically ordered ground state. However, recent scanning tunneling measurements [27–29] in MLG find charge-ordered ground states

at $\nu=0$, with a Kekule bond-order (BO) or a charge density wave (CDW) order. Given the difficulty in reconciling these conflicting observations (within the OM), recently one of us [30, 31] reevaluated the $\nu=0$ phase diagram allowing the lattice-scale interactions to assume a more generic form. These studies find that coexistence phases with both spin and charge order may appear if interactions have a structure at the scale of ℓ .

As a matter of principle, and irrespective of specific filling factor and device details, the phenomenological terms in the low energy model may have a complicated form due to quantum fluctuations involving other (positive and negative energy) LLs [32–36]. This LL mixing is largely controlled by the parameter $\kappa = E_c/\hbar\omega_c$, the ratio of the Coulomb energy scale (E_c) to the cyclotron gap $(\hbar\omega_c)$ [34]. In general, LL mixing introduces a nontrivial component with a range of ℓ to the effective interactions, which may be attractive or repulsive. Moreover, the B-dependence of these terms may be different from that of the bare terms. Refs. 30 and 31 demonstrate that such considerations not only affect the energetics, but also add to the set of possible ground states [37].

In this Letter, we explore the QH phases of BLG and provide further evidence for the crucial role of such modified interactions. We consider a dual-gated device, which allows the application of a transverse electric field (D) as an experimental knob to tune between different ground states at fixed filling factor ν . Close to charge neutrality, the chemical potential lies within a set of eight (nearly) degenerate LLs labelled by spin, valley and an orbital index, supporting a variety of brokensymmetry states in the range $|\nu| < 4$. Indeed, transport [23, 40–42] and capacitance [43] measurements provide evidence for a complex sequence of phase transitions driven by D for both integer and fractional fillings. The number of transitions and the values of D at which

they occur are functions of ν and B. As shown below, the complete phase diagram in the $\{D, B, \nu\}$ space encodes vital information on the underlying many-body effects.

Notably, the OM is consistent with many earlier measurements, restricted to certain regions of the parameter space such as a fixed value of B [43] or integer ν [41]. Our present study is based on transport measurements over a wide range of parameters, including moderate and high B, where experimental data in higher-quality samples are now available. Specifically, we focus on filling factors $1 < \nu \le 2$, and track the variation of the critical electric field (D^*) at which a phase transition occurs with B and ν [Fig. 1]. We find that $D^*(\nu)$ is an increasing (decreasing) function of ν at high (low) B-fields, and that D^* may even vanish at sufficiently low fields. It is worth emphasizing that because the chemical potential is pinned to the same LL for this filling factor range, the behavior of $D^*(\nu, B)$ is controlled by the lattice-scale interactions, and imposes significant constraints on their form. The elucidation of these interactions is the main purpose of this work.

The main finding of this Letter is that the OM of lattice-scale interactions cannot account for the observed behavior of $D^*(\nu, B)$. Our Hartree-Fock (HF) analysis demonstrates that the symmetry-breaking interactions must have both repulsive and attractive components with different B-dependence in order to explain the measurements [Fig. 2]. These results suggest that corrections arising from the LL-mixing play a significant role in BLG, particularly at lower B. We further employ this model to construct the phase diagram of the $\nu = 2$ QH state in the B-D plane [Fig. 3]. Interestingly, we find the emergence of an inter-orbital valley-coherent phase around $D \sim D^*$ for sufficiently large B. The existence of such a valley-orbital entangled (VOE) phase at high B implies that the transport gap at $\nu = 2$ does not close around $D = D^*$. Additionally, valley-coherence points to the presence of a Kekule BO phase which may be observed in tunnelling measurements, similar to those reported in Refs. 27–29.

Transport Measurements. We employ a high quality dual-gated BLG device, device 002, described previously in Ref. 42, to examine the behavior of D^* as a function of B at different filling factors. Figure 1(a) shows a color map of $R_{xx}(D)$ in the range $1 < \nu < 2$ at B = 18 T and T = 20 mK (See the full dataset covering a wider range of ν in Ref. 42). Regions with darker colors correspond to vanishingly small R_{xx} indicating QH phases. The black dashed curve marks the true inversion symmetric line, i.e. where D=0 is. Device asymmetry causes a slight asymmetry between D_{+}^{*} and D_{\neg}^{*} (the red dashed lines), where two (non-interacting) LLs with different valley and orbital indices cross [41], as depicted in the inset of Fig. 1(c). Figure 1(b) depicts traces of $R_{xx}(D)$ at B=28 T and T=0.33 K for different ν . D_{\neg}^* manifests as resistance peaks marked by *. Figure 1(d) plots $R_{xx}(D)$ for $\nu = 2$ at different B taken at T = 3 K, where D_{+}^{*} (marked by *) become more readily observ-

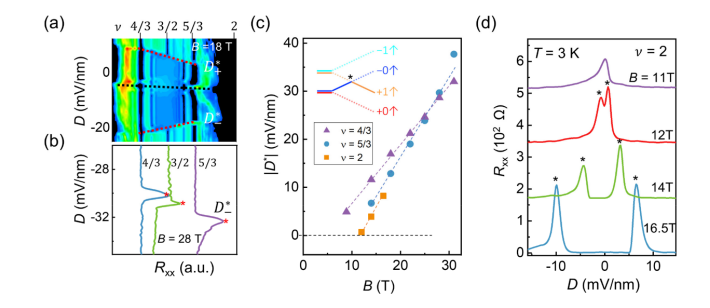


FIG. 1. (a) False color map of $R_{xx}(\nu, D)$ between $\nu=1$ and 2 at B=18 T (obtained in Ref. [42]). The red dashed lines mark the positive and negative critical electric fields (D_{\pm}^*) , at which a first-order phase transition, as illustrated in the inset of (c), occurs. The black dashed line marks the true D=0. (b) Line scans of R_{xx} vs D obtained at fixed $\nu=4/3$ (blue), 3/2 (green) and 5/3 (violet) at B=28 T. The resistance peaks (marked by *) correspond to D_{-}^* . Note that $|D^*|$ increases/decreases with ν at B=28/18 T. (c) B-field dependence of D^* for different ν . Dashed lines are guide to the eye. (d) Line scans of R_{xx} vs D for $\nu=2$ at different B. The transitions D_{\pm}^* are marked by *. The average of D_{\pm}^* at $\nu=2$ is plotted as squares in (c). D_{-}^* for $\nu=4/3$ (5/3) are obtained using similar measurements and shown as triangles (circles). All data are from device 002.

able for $\nu = 2$. The closing of the transport gap signals a first order phase transition, similar to previous observations in GaAs [44], the position of which evolves with B. Figure 1(c) depicts the evolution of D^* with B for $\nu = 2,5/3$ and 4/3 obtained through a similar analysis.

A salient feature of the color map [Fig. 1(a)] is that at B = 18 T, D^* (defined as the average of $|D_+^*|$) is monotonically decreasing with increasing ν . This is not always the case: Figure 1(b) shows that D^* increases with increasing ν at B=28 T. This change of behavior is illustrated in Fig. 1(c), which shows the variation of D^* with B for different values of ν . Strikingly, the various curves appear to cross around $B = B_s \sim 26 \text{ T}$, implying that $D^*(\nu)$ is an increasing (decreasing) function of ν for $B > B_s$ ($B < B_s$). Furthermore, $D^*(\nu)$ decreases monotonically upon lowering B and appears to vanish for sufficiently small B. For example, $D^*(\nu=2)$ vanishes at $B = B_* \sim 11$ T. This can be seen clearly in Fig. 1(d), where the two resistance peaks observed for at higher B (which mark D_+^*) merge into one at $B = B_* \sim 11 \text{ T, implying } D_+^* = D_-^* = 0.$

The theoretical challenge here is to account for the two most prominent features observed in the data: (a) the change in the slope of D^* vs ν from positive for $B > B_s$ to negative for $B < B_s$, and (b) the vanishing of $D^*(\nu = 2)$ at $B = B_*$. A subsidiary puzzle is the nature of the $\nu = 2$ ground state as D is tuned close to D^* . Additionally, the theoretical model has to be consistent with previous observations at $\nu = 0$, such as the canted antiferromagnet and layer polarized phases.

Theoretical Model. The LL spectrum of BLG close to charge neutrality (chemical potential $|\mu| \ll \hbar \omega_c$) consists of eight nearly degenerate LLs, corresponding to

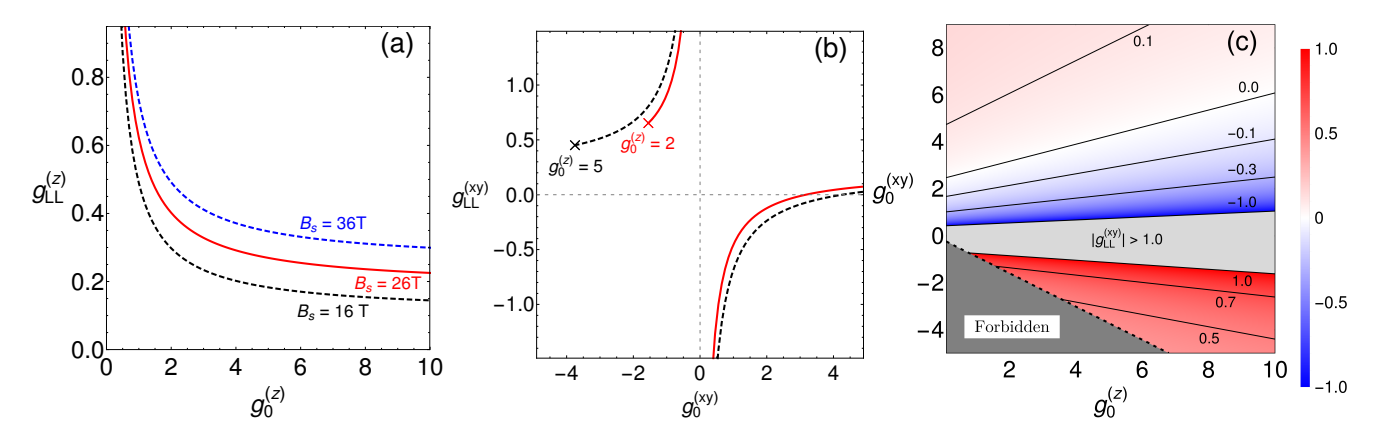


FIG. 2. Constraints on the interactions $v_i(q)$ [i=z,xy] dictated by transport measurements. The parameters $g_0^{(i)}$, $g_{LL}^{(i)}$, ξ are defined in Eq. 3. (a) $g_{LL}^{(z)}$ as a function of $g_0^{(z)}$ for different B_s (the field at which the slope of D^* vs ν changes sign). Consistency with experiments rules out negative values of $g_0^{(z)}$. (b) $g_{LL}^{(xy)}$ versus $g_0^{(xy)}$ for different values of $g_0^{(z)}$. The cross marks the smallest value of $g_0^{(xy)}$ at which the theoretical model remains consistent with experiments. Notably, v_z and v_{xy} may comprise both repulsive and attractive components. (c) Contour plot of $g_{LL}^{(xy)}$ in the $g_0^{(z)} - g_0^{(xy)}$ plane. The dark gray region (below the dashed curve) is forbidden by experimental constraints. Here, we used $\xi = 0.3$ and $\epsilon = 6$. In (b) and (c) we used $B_s = 26$ T and $B_* = 11$ T.

the spin, valley and orbital degrees of freedom. Experimental evidence, e.g. the absence of any dependence on the in-plane field in the activation energy gaps measured at $\nu=2,3$ [19] and the relatively large effective Zeeman coupling [41], indicate that in the filling factor range of interest to us $(\nu\sim2)$ the electronic states are spin-polarized. We therefore restrict the Hilbert space in the model to four LLs, labelled by the orbital (N=0,1) and valley $(\alpha=\pm)$ indices. The two orbitals are not degenerate as there is no symmetry relating them. On the other hand, the two valleys are degenerate unless inversion symmetry is broken by a perpendicular electric field D (or sublattice potentials, which are ignored here). The one-body part of the Hamiltonian is hence given by $H_0 = \sum_{N\alpha k} \epsilon_{\alpha N} c_{N\alpha k}^{\dagger} c_{N\alpha k}$, where k is the guiding center index in the Landau gauge, and

$$\epsilon_{\alpha N} = N\Delta_{10} + \alpha \frac{\Delta_D}{2} |\mathcal{P}_{N\alpha}|.$$
 (1)

Here Δ_{10} is the energy gap between the two orbitals (for D=0), $\mathcal{P}_{N\alpha}$ is the layer polarization, and $\Delta_D \propto D$ is the interlayer potential difference generated by D.

To evaluate the energies and wave functions of the (non-interacting) states, we employed an effective four-band model (corresponding to the four sites of the unit-cell) [45], which includes all tight-binding parameters found to be finite in ab-initio studies [46]. In particular, our model incorporates both trigonal warping and the hopping between Bernal-stacked sites exactly (see Ref. 47 for details). Ignoring the Bernal-sites leads to perfect valley-layer locking, such that $\mathcal{P}_{N\alpha} = \alpha$. By contrast, in the full 4-component spinor the weight on these sites increases with B and $\mathcal{P}_{N\alpha}$ depends on N [43]. This orbital dependence has significant impact on the variation of D^* . Trigonal warping modifies the density profile of the wave functions at each site, which affects

the interaction matrix elements and plays an important role in stabilizing novel ground states (see e.g. Ref. 18).

The interacting part of the Hamiltonian comprises two components, H_c and H_v . H_c is an SU(4) symmetric (screened Coulomb) density-density interaction. The (Fourier transformed) pair potential for this is $v_c(q) = \frac{E_c}{\epsilon} v_{\rm eff}(q)$, where $E_c = \frac{e^2}{4\pi\epsilon_0} \frac{1}{\ell}$ is the Coulomb energy scale, ϵ is the relative permittivity of hBN, and $v_{\rm eff}(q) = f(q)/q\ell$ where f(q) is a form factor that accounts for screening from the top and bottom gates as well as higher energy LLs (at the RPA level) [47]. H_v represents the lattice-scale corrections, which reduce the valley symmetry to $U(1) \times \mathbb{Z}_2$. We assume that these corrections do not depend on the orbitals, and only include the terms present in the Kharitonov model of BLG [15, 16] which may be expressed as

$$2\pi\ell^2 \times \frac{1}{2A} \sum_{i=x,y,z} \sum_{\vec{q}} v_i(q) : \rho_i(\vec{q}) \rho_i(-\vec{q}) :, \qquad (2)$$

where A is the area of the sample, and $\rho_i(q)$ the (Fourier transform of) i^{th} component of local isospin density [47]. Valley U(1) symmetry leads to $v_x(q) = v_y(q) \equiv v_{xy}(q)$. While $v_i(q)$ (i = z, xy) is replaced by a constant in the OM, here we assume the more general form,

$$v_i(q) = g_0^{(i)} \times \left(E_c \frac{a}{\ell} \right) \left[1 - g_{LL}^{(i)} \times \kappa \times e^{-\frac{\xi}{2}(q\ell)^2} \right]$$
 (3)

where a is the lattice constant. In the limit $\kappa \to 0$, $v_i(q)$ reduces to the standard short-range form with strength $g_0^{(i)}\left(E_c\frac{a}{\ell}\right) \propto B$. For finite κ the second term of (3), which phenomenologically models corrections due to LL mixing, becomes progressively more important, with the characteristic scale $\kappa \times \left(E_c\frac{a}{\ell}\right) \propto \sqrt{B}$. We emphasize that the two components of $v_i(q)$ differ not just in their range, but crucially also in their dependence on B, and

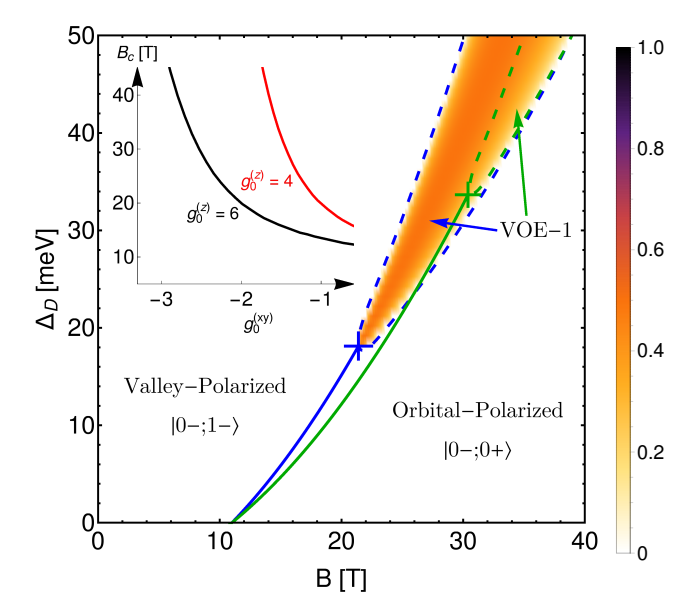


FIG. 3. Phase diagram at $\nu=2$. The solid lines mark a first order transition between the valley-polarized and orbital-polarized phases (corresponding to D^*); the blue (green) curves correspond to $g_0^{(xy)}=-2.0$ ($g_0^{(xy)}=-2.5$). The plus signs (at $B=B_c\sim 20T$ and 30T) mark a critical point where the first order phase boundary terminates. The dashed lines at higher B mark the region where an intervening valley-orbital entangled phase (denoted by VOE-1) emerges around D^* , which allows for a continuous transition between the two polarized phases. The color map shows the variation of the order parameter $\langle \eta_x \rangle$ in the VOE-1 phase (see text) for $g_0^{(xy)}=-2.0$. The VOE-1 phase is characterized by a density matrix with the form in (5) with $\theta_A\in(0,\pi)$ and $\theta_B=0$. The inset shows the variation of B_c (the field at which the first order transition ends) with $g_0^{(xy)}$ for different $g_0^{(z)}$. Here, we used $\epsilon=6$, $\xi=0.3$ and $g_0^{(z)}=6.0$. $g_{LL}^{(i)}$ were chosen such that $B_s=26$ T and $B_*=11$ T.

may have different signs. The dimensionless numbers $g_0^{(i)},\ g_{LL}^{(i)}$ and $\xi,$ assumed to be independent of B, are the tuning parameters of the model.

We treat the interactions in the self-consistent HF approximation. The HF ground state, assumed to be translationally invariant, is characterized by the single-particle averages $\langle c_{N_1\alpha_1k_1}^{\dagger}c_{N_2\alpha_2k_2}\rangle = \delta_{k_1k_2}\Delta_{N_2\alpha_2}^{N_1\alpha_1}$, which minimize the variational energy. All details (including the B dependence) of the interaction potentials and the single-particle wave functions are folded into the set of Hartree and Fock couplings [47].

Variation of D^* . The $\nu=2$ ground state corresponds to complete filling of two of the four LLs included in the model. Equation (1) suggests that the (non-interacting) ground state is $|0-,0+\rangle \equiv \Pi_k c_{0-k}^{\dagger} c_{0+k}^{\dagger} |0\rangle$ for $D\sim 0$ and a valley polarized phase $|0-,1-\rangle$ at large (and positive) D. The transition occurs at $D=D^*(\nu=2)$ for which the energy of the two states is equal. Comparing the HF variational energy of these two states leads to an analytic equation for $D^*(\nu=2)$ [47].

Upon reducing the filling factor to $\nu=2-\delta\nu$, the highest energy occupied LL is partially depleted. For $\delta\nu\ll 1$ this yields a linear equation $D^*(2-\delta\nu)=D^*(2)-m_{D^*}\delta\nu$, where, up to an unimportant prefactor, the slope of D^* vs ν (m_{D^*}) is

$$m_{D^*} = \left(\mathcal{F}_{0000}^{(c)} - \mathcal{F}_{1111}^{(c)}\right) + \left(\mathcal{F}_{0000}^{(z)} - \mathcal{F}_{1111}^{(z)}\right).$$
 (4)

Here $\mathcal{F}_{NNNN}^{(i)}$ is the Fock integral for Coulomb (i=c) and v_z (i=z) interactions which couples electrons within one of the $|N,\alpha\rangle$ LL's [47]. For repulsive interactions $\mathcal{F}_{0000} \geq \mathcal{F}_{1111}$ since the N=0 states are more localized than those with N=1. Hence, $m_{D^*}>0$ for all B if only Coulomb interactions are present. In order to account for the experimental observations, $\mathcal{F}_{0000}^{(z)} - \mathcal{F}_{1111}^{(z)}$ must be sufficiently negative at $B < B_s$ and positive at higher B. We find that this cannot be achieved without a finite $g_{LL}^{(z)}$ [Fig. 2(a)]. Our measurements constrain both $g_0^{(z)}$ and $g_{LL}^{(z)}$ to be positive, suggesting that v_z must have both short-ranged repulsive and longer-ranged attractive components.

Next, we turn to the vanishing of $D^*(\nu=2)$ at $B=B_*\sim 11$ T. This can be achieved for generic values of $g_0^{(z)}$ and $g_0^{(xy)}$, if $g_{LL}^{(xy)}$ is also finite [Figs. 2(b,c)]. Interestingly, the experimental results also constrain the possible values of the bare lattice interaction parameters $(g_0^{(z)}$ and $g_0^{(xy)})$. Specifically, $g_0^{(z)}$ may only assume positive values, while $g_0^{(xy)}$ must be larger than a certain cutoff [Fig. 2(c)].

Intervalley Coherence. The analysis thus far considered ground states for which α and N are good quantum numbers. Since two LLs with different valley and orbital indices are nearly degenerate in the $D \sim D^*$ regime, the system may be able to lower the variational energy by hybridizing these LLs and forming a more complex ground state. We performed unrestricted HF calculations over a wide range of parameters to explore the nature of the $\nu = 2$ phase. This analysis uncovered a rich variety of possible ground states involving hybridization between different pairs of LLs [47]. Here, we restrict the range of parameters to $g_0^{(z)} > 0$ and $g_0^{(xy)} < 0$, which is consistent with previous studies at $\nu = 0$ in this system [21, 23, 26]. In this regime, the state is well-described for all B, D by an ansatz for $\Delta_{N_2\alpha_2}^{N_1\alpha_1}$ of the form

$$\frac{1}{2} \begin{pmatrix}
1 + \cos(\theta_A) & 0 & \sin(\theta_A) \\
0 & 1 + \cos(\theta_B) & \sin(\theta_B) & 0 \\
0 & \sin(\theta_B) & 1 - \cos(\theta_B) & 0 \\
\sin(\theta_A) & 0 & 0 & 1 - \cos(\theta_A)
\end{pmatrix}$$
(5)

in the $(N\alpha)=(0+,0-,1+,1-)$ basis. The angles $\theta_{A,B}\in[0,\pi]$ parameterize the state [55]. The orbital-(valley-)polarized state is described by $\theta_A=\theta_B=0$ ($\theta_A=\pi,\ \theta_B=0$). $\theta_{A,B}\neq 0,\pi$ correspond to interorbital valley-coherent phases which smoothly interpolate between the two polarized states. These VOE

phases break the U(1)-valley symmetry and are characterized by the order parameter $\langle \eta_x \rangle = \frac{1}{2} \left[\sin(\theta_A) + \frac{1}{2} \right]$ $\sin(\theta_B)$]. Our analysis finds that for generic parameters (consistent with experiments), the polarized phases are separated by a first order transition for low values of B. The first order boundary terminates at a certain magnetic field, and a VOE phase appears in a finite parameter range around $D = D^*$ for higher values of B (Fig. 3 shows a typical phase diagram). We refer to this phase as VOE-1 because (generically) valley coherence emerges only in one of the sectors, i.e., $\theta_B = 0$ and $\theta_A \in (0,\pi)$ for D > 0. Such a valley coherent phase may exhibit Kekule BO. At the lattice scale these phases break translational symmetry, but upon coarsegraining to the scale ℓ , they do not, in accordance with our original assumptions regarding Δ .

Discussion. The results presented above rely on the HF approximation, which ignores the effect of quantum fluctuations and correlations (beyond exchange). However, we believe that the qualitative features of our results would remain unaltered even when these effects are included. The cornerstone of our analysis is the distinct behavior of $D^*(\nu)$ at low and high B-fields. Our measurements show that $D^*(\nu)$ is a relatively smooth function for $1 < \nu \le 2$. By contrast, correlation effects, which are crucial in stabilizing fractional QH phases, strongly depend on the precise value of ν and may be wildly different even for nearby fractions. This indicates that such effects do not play an important role in determining the qualitative behavior of $D^*(\nu)$ over a broad range of filling factors, which is apparently well-captured by the HF approximation. We emphasize that correlations beyond HF do affect $D^*(\nu, B)$ quantitatively, even at higher B [43].

Our model further accounts for the vanishing of $D^*(\nu=2)$ at $B=B_*$. Its experimental value $(B_*\sim 11\,\mathrm{T})$ allows us to constrain two of the four tuning parameters in the model, the couplings of the components arising from LL mixing $(g_{\rm LL})$. The fact that even the qualitative behavior of the measured D^* cannot be explained without finite $g_{\rm LL}$ strongly implies that LL-mixing plays a crucial role in determining the ground state, by introducing a effective attractive interactions that scale differently with B. These interactions become particularly pronounced at low B.

We note that the U(1) valley symmetry is an artifact of the continuum approximation, and the restriction to just two-body interactions. LL mixing would not only modify the two-body potential, but also introduce three and higher-body terms. Since $3(\vec{K} - \vec{K}')$ (where \vec{K} and \vec{K}' are the locations of the valley centers in the Brillouin zone) is a reciprocal lattice vector, the lattice translation symmetry allows for three-body Umklapp terms transferring 3 fermions from one valley to the other. These terms reduce the U(1) symmetry, associated with the conservation of the difference of charge between the valleys, to \mathbb{Z}_3 . Hence, the valley-coherent phase breaks a discrete symmetry, and may exist at finite temperatures. In fact, it corresponds to a Kekule bond-ordered phase, similar to those observed in STM experiments on MLG recently [27–29].

Conclusions. Using high-quality BLG devices, we explored the behavior of the critical electric field $D^*(\nu, B)$ in the range $1 < \nu \le 2$, and observed a qualitative difference between the high and low B regimes. Remarkably, we found that the standard theoretical models of BLG are not consistent with these measurements. Instead, it is crucial to consider the corrections to the lattice-scale interactions arising from LL-mixing, which we argued lead to an effective attraction at short but finite length scales. We presented a phenomenological model of these which accounts for the experiments. It moreover predicts an inter-orbital valley-coherent phase for $D \sim D^*$ at high B, which may be observed as a bond-ordered state in STM experiments. Our work motivates a detailed theoretical analysis of the LL-mixing corrections to lattice-scale interactions in MLG and BLG. Their effect on other integer and fractional QH states is another interesting direction for future investigations.

Acknowledgements. We thank Chunli Huang, Ribhu Kaul and Benjamin Sacepe for useful discussions. ES, HAF and GM thank the Aspen Center for Physics (NSF) Grant No. 1066293) for its hospitality, and financial support by the US-Israel Binational Science Foundation through award No. 2016130. UK and ES acknowledge the support of the US-Israel Binational Science Foundation through award No. 2018726, and the Israel Science Foundation (ISF) Grant No. 993/19. HAF acknowledges the support of the NSF through Grant Nos. ECCS-1936406 and DMR-1914451. KH and JZ acknowledge support from the National Science Foundation through Grant No. NSF-DMR-1904986. The experiments were performed at the National High Magnetic Field Laboratory which was supported by the National Science Foundation through Grant No. NSF-DMR-1644779 and the State of Florida. KW and TT acknowledge support from JSPS KAKENHI (Grant Nos. 19H05790, 20H00354 and 21H05233).

^[1] R. E. Prange and S. M. Girvin, eds., *The Quantum Hall Effect* (Springer New York, 1990).

^[2] S. D. Sarma and A. Pinczuk, eds., Perspectives in Quantum Hall Effects (Wiley New York, 1997).

^[3] Z. F. Ezawa, Quantum Hall Effects (World Scientific, 2008).

^[4] B. I. Halperin and J. Jain, eds., Fractional Quan-

tum Hall Effects: New Developments (World Scientific, 2020).

^[5] S. A. Parameswaran and B. E. Feldman, Quantum Hall valley nematics, J. Phys.: Condens. Matter 31, 273001 (2019).

^[6] A. H. Castro Neto, F. Guinea, N. M. R. Peres, K. S. Novoselov, and A. K. Geim, The electronic properties

- of graphene, Rev. Mod. Phys. 81, 109 (2009).
- [7] K. Yang, S. Das Sarma, and A. H. MacDonald, Collective modes and skyrmion excitations in graphene SU(4) quantum Hall ferromagnets, Phys. Rev. B 74, 075423 (2006).
- [8] Y. Zhang, Z. Jiang, J. P. Small, M. S. Purewal, Y.-W. Tan, M. Fazlollahi, J. D. Chudow, J. A. Jaszczak, H. L. Stormer, and P. Kim, Landau-level splitting in graphene in high magnetic fields, Phys. Rev. Lett. 96, 136806 (2006).
- [9] Z. Jiang, Y. Zhang, H. L. Stormer, and P. Kim, Quantum Hall states near the charge-neutral Dirac point in graphene, Phys. Rev. Lett. 99, 106802 (2007).
- [10] Y. L. and Jairo Velasc and David Tran and Fan Zhang and W. Bao and Lei Jing and Kevin Myhro and Dmitry Smirnov and Chun Ning Lau, Broken symmetry quantum Hall states in dual-gated aba trilayer graphene, Nano Lett. 13, 1627 (2013).
- [11] B. Datta, S. Dey, A. Samanta, H. Agarwal, A. Borah, K. Watanabe, T. Taniguchi, R. Sensarma, and M. M. Deshmukh, Strong electronic interaction and multiple quantum Hall ferromagnetic phases in trilayer graphene, Nature Communications 8, 14518 (2017).
- [12] S. Che, Y. Shi, J. Yang, H. Tian, R. Chen, T. Taniguchi, K. Watanabe, D. Smirnov, C. N. Lau, E. Shimshoni, G. Murthy, and H. A. Fertig, Helical edge states and quantum phase transitions in tetralayer graphene, Phys. Rev. Lett. 125, 036803 (2020).
- [13] J. Alicea and M. P. A. Fisher, Graphene integer quantum Hall effect in the ferromagnetic and paramagnetic regimes, Phys. Rev. B 74, 075422 (2006).
- [14] M. Kharitonov, Phase diagram for the $\nu=0$ quantum Hall state in monolayer graphene, Phys. Rev. B 85, 155439 (2012).
- [15] M. Kharitonov, Canted antiferromagnetic phase of the ν =0 quantum Hall state in bilayer graphene, Phys. Rev. Lett. 109, 046803 (2012).
- [16] M. Kharitonov, Antiferromagnetic state in bilayer graphene, Phys. Rev. B 86, 195435 (2012).
- [17] B. Feshami and H. A. Fertig, Hartree-fock study of the $\nu=0$ quantum Hall state of monolayer graphene with short-range interactions, Phys. Rev. B **94**, 245435 (2016).
- [18] G. Murthy, E. Shimshoni, and H. A. Fertig, Spin-valley coherent phases of the $\nu=0$ quantum Hall state in bilayer graphene, Phys. Rev. B **96**, 245125 (2017).
- [19] Y. Zhao, P. Cadden-Zimansky, Z. Jiang, and P. Kim, Symmetry breaking in the zero-energy Landau level in bilayer graphene, Phys. Rev. Lett. 104, 066801 (2010).
- [20] A. F. Young, C. R. Dean, L. Wang, H. Ren, P. Cadden-Zimansky, K. Watanabe, T. Taniguchi, J. Hone, K. L. Shepard, and P. Kim, Spin and valley quantum Hall ferromagnetism in graphene, Nature Physics 8, 550 (2012).
- [21] P. Maher, C. R. Dean, A. F. Young, T. Taniguchi, K. Watanabe, K. L. Shepard, J. Hone, and P. Kim, Evidence for a spin phase transition at charge neutrality in bilayer graphene, Nature Physics 9, 154 (2013).
- [22] A. F. Young, J. D. Sanchez-Yamagishi, B. Hunt, S. H. Choi, K. Watanabe, T. Taniguchi, R. C. Ashoori, and P. Jarillo-Herrero, Tunable symmetry breaking and helical edge transport in a graphene quantum spin Hall state, Nature 505, 528 (2014).
- [23] J. Li, H. Fu, Z. Yin, K. Watanabe, T. Taniguchi, and J. Zhu, Metallic phase and temperature dependence of

- the $\nu = 0$ quantum Hall state in bilayer graphene, Phys. Rev. Lett. **122**, 097701 (2019).
- [24] D. S. Wei, T. van der Sar, S. H. Lee, K. Watanabe, T. Taniguchi, B. I. Halperin, and A. Yacoby, Electrical generation and detection of spin waves in a quantum Hall ferromagnet, Science 362, 229 (2018).
- [25] P. Stepanov, S. Che, D. Shcherbakov, J. Yang, R. Chen, K. Thilahar, G. Voigt, M. W. Bockrath, D. Smirnov, K. Watanabe, T. Taniguchi, R. K. Lake, Y. Barlas, A. H. MacDonald, and C. N. Lau, Long-distance spin transport through a graphene quantum Hall antiferromagnet, Nature Physics 14, 907 (2018).
- [26] H. Fu, K. Huang, K. Watanabe, T. Taniguchi, and J. Zhu, Gapless spin wave transport through a quantum canted antiferromagnet, Phys. Rev. X 11, 021012 (2021).
- [27] S.-Y. Li, Y. Zhang, L.-J. Yin, and L. He, Scanning tunneling microscope study of quantum Hall isospin ferromagnetic states in the zero Landau level in a graphene monolayer, Phys. Rev. B 100, 085437 (2019).
- [28] A. Coissard, D. Wander, H. Vignaud, A. G. Grushin, C. Repellin, K. Watanabe, T. Taniguchi, F. Gay, C. B. Winkelmann, H. Courtois, H. Sellier, and B. Sacepe, Imaging tunable quantum Hall broken-symmetry orders in graphene, Nature 605, 51 (2022).
- [29] X. Liu, G. Farahi, C.-L. Chiu, Z. Papic, K. Watanabe, T. Taniguchi, M. P. Zaletel, and A. Yazdani, Visualizing broken symmetry and topological defects in a quantum Hall ferromagnet, Science 375, 321 (2022).
- [30] A. Das, R. K. Kaul, and G. Murthy, Coexistence of canted antiferromagnetism and bond order in $\nu = 0$ graphene, Phys. Rev. Lett. 128, 106803 (2022).
- [31] S. J. De, A. Das, S. Rao, R. K. Kaul, and G. Murthy, Global phase diagram of charge-neutral graphene in the quantum Hall regime for generic interactions, Phys. Rev. B 107, 125422 (2023).
- [32] G. Murthy and R. Shankar, Hamiltonian theory of the fractional quantum Hall effect: Effect of Landau level mixing, Phys. Rev. B 65, 245309 (2002).
- [33] W. Bishara and C. Nayak, Effect of Landau level mixing on the effective interaction between electrons in the fractional quantum Hall regime, Phys. Rev. B 80, 121302 (2009).
- [34] M. R. Peterson and C. Nayak, More realistic Hamiltonians for the fractional quantum Hall regime in GaAs and graphene, Phys. Rev. B 87, 245129 (2013).
- [35] I. Sodemann and A. H. MacDonald, Landau level mixing and the fractional quantum Hall effect, Phys. Rev. B 87, 245425 (2013).
- [36] S. H. Simon and E. H. Rezayi, Landau level mixing in the perturbative limit, Phys. Rev. B 87, 155426 (2013).
- [37] Finite-ranged interactions were also employed in Ref. 38 in the context of $\nu=\pm 1$ phases of MLG. Finite-ranged terms emerge naturally upon projection of short-ranged interactions in a set of finite energy $(N \neq 0)$ LLs [39].
- [38] J. Atteia and M. O. Goerbig, Su(4) spin waves in the $\nu=\pm 1$ quantum Hall ferromagnet in graphene, Phys. Rev. B **103**, 195413 (2021).
- [39] N. Stefanidis and I. S. Villadiego, Competing spin-valley entangled and broken symmetry states in the N=1 Landau level of graphene, Phys. Rev. B **107**, 045132 (2023).
- [40] P. Maher, L. Wang, Y. Gao, C. Forsythe, T. Taniguchi, K. Watanabe, D. Abanin, Z. Papić, P. Cadden-

- Zimansky, J. Hone, P. Kim, and C. R. Dean, Tunable fractional quantum Hall phases in bilayer graphene, Science **345**, 61 (2014).
- [41] J. Li, Y. Tupikov, K. Watanabe, T. Taniguchi, and J. Zhu, Effective Landau level diagram of bilayer graphene, Phys. Rev. Lett. 120, 047701 (2018).
- [42] K. Huang, H. Fu, D. R. Hickey, N. Alem, X. Lin, K. Watanabe, T. Taniguchi, and J. Zhu, Valley isospin controlled fractional quantum Hall states in bilayer graphene, Phys. Rev. X 12, 031019 (2022).
- [43] B. M. Hunt, J. I. A. Li, A. A. Zibrov, L. Wang, T. Taniguchi, K. Watanabe, J. Hone, C. R. Dean, M. Zaletel, R. C. Ashoori, and A. F. Young, Direct measurement of discrete valley and orbital quantum numbers in bilayer graphene, Nature Communications 8, 948 (2017).
- [44] E. P. D. Poortere, E. Tutuc, S. J. Papadakis, and M. Shayegan, Resistance spikes at transitions between quantum Hall ferromagnets, Science 290, 1546 (2000).
- [45] E. McCann and V. I. Falko, Landau-level degeneracy and quantum Hall effect in a graphite bilayer, Phys. Rev. Lett. 96, 086805 (2006).
- [46] J. Jung and A. H. MacDonald, Accurate tight-binding models for the π bands of bilayer graphene, Phys. Rev. B 89, 035405 (2014).
- [47] See Supplemental Material for additional details regarding our theoretical analysis. The Supplemental Material includes Refs. [48–54].
- [48] E. McCann and M. Koshino, The electronic properties

- of bilayer graphene, Rep. Prog. Phys. **76**, 056503 (2013).
- [49] N. Ohba, K. Miwa, N. Nagasako, and A. Fukumoto, First-principles study on structural, dielectric, and dynamical properties for three BN polytypes, Phys. Rev. B 63, 115207 (2001).
- [50] F. Yang, A. A. Zibrov, R. Bai, T. Taniguchi, K. Watanabe, M. P. Zaletel, and A. F. Young, Experimental determination of the energy per particle in partially filled Landau levels, Phys. Rev. Lett. 126, 156802 (2021).
- [51] E. V. Gorbar, V. P. Gusynin, and V. A. Miransky, Dynamics and phase diagram of the $\nu=0$ quantum Hall state in bilayer graphene, Phys. Rev. B **81**, 155451 (2010).
- [52] E. V. Gorbar, V. P. Gusynin, V. A. Miransky, and I. A. Shovkovy, Broken symmetry $\nu=0$ quantum Hall states in bilayer graphene: Landau level mixing and dynamical screening, Phys. Rev. B 85, 235460 (2012).
- [53] Z. Papic and D. A. Abanin, Topological phases in the zeroth Landau level of bilayer graphene, Phys. Rev. Lett. 112, 046602 (2014).
- [54] K. Snizhko, V. Cheianov, and S. H. Simon, Importance of interband transitions for the fractional quantum Hall effect in bilayer graphene, Phys. Rev. B 85, 201415 (2012).
- [55] In principle, the ansatz allows for an additional parameter corresponding to the relative phase between A and B sectors. Here, we ignore this phase as it drops out of the energy functional [47].